Mesoscale Two-Photon Microscopy: Engineering a Wide Field of View with Cellular Resolution

Jeffrey N. Stirman, PhD, and Spencer L. Smith, PhD

Neuroscience Center and Department of Cell Biology and Physiology
University of North Carolina at Chapel Hill
Chapel Hill, North Carolina

Introduction

Information is widely distributed in neuronal networks. Patterns of activity across multiple brain areas act in concert to support sensory processing and behavior. Mapping this activity with cellular resolution can reveal principles of neural function but presents technical challenges.

Electrodes offer unsurpassed temporal resolution and can easily record from spatially separate populations. However, this approach is invasive, cannot be genetically targeted to record from specific cell types, and only sparsely samples local populations. By contrast, two-photon imaging of free calcium is less invasive, can be genetically targeted, and offers dense sampling of local populations. Two-photon imaging (Denk et al., 1990) is particularly suited for imaging activity in highly scattering neuropil, such as mammalian cortex, and the latest generation of genetically encoded calcium indicators (GECIs) can provide a high-fidelity optical readout of spiking (Chen et al., 2013).

However, conventional implementations of two-photon microscopy are often limited in their primary field of view (FOV) to approximately 700 µm. Outside of this region, limiting apertures and aberrations decreases the effectiveness of two-photon excitation, leading to dim regions ("vignetting") and reduced resolution. Brain regions can be distributed over areas larger than this FOV. For example, cortical areas in mice are distributed over millimeters of cortex (Fig. 1). Thus, engineering improvements are needed to enable two-photon microscopy of FOVs large enough to encompass multiple brain regions. We refer to this wide FOV imaging as "mesoscale two-photon imaging."

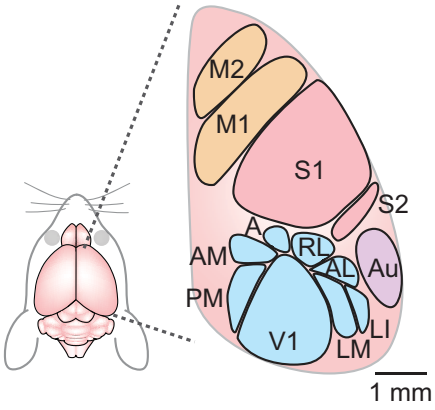

Figure 1. Imaging multiple cortical areas in a mouse requires an FOV that spans >1 mm (scale bar). Schematic layout of a selection of cortical areas in the mouse. Primary visual cortex (V1, shaded blue) and higher visual areas (A, anterior; AL, anterolateral; AM, anteromedial; LI, laterointermediate; LM, lateromedial; PM, posteromedial; and RL, rostrolateral, all shaded blue); auditory cortex (Au, shaded violet); primary and secondary sensory cortex (S1, S2, shaded pink); and primary and secondary motor cortex (M1, M2, shaded orange). Many cortical areas are >0.5 mm wide, and thus a FOV >1 mm wide is required to simultaneously image neurons in multiple cortical areas beyond immediate boundary regions.

In this chapter, we discuss the main factors that limit the FOV of two-photon imaging and how to engineer optimized implementations to retain cellular resolution across a large FOV. We will also discuss imaging speed, which is crucial to ensure temporal resolution sufficient to map neural activity on timescales that are relevant for coding and behavior.

Optomechanical Considerations

There are three main optomechanical determinants of the FOV for a laser scanning microscope: the scan angles (SAs) of the beam scanning engine (SE) (e.g., galvanometer mirrors); the magnification of the beam expansion relay (the ratio of the focal lengths of the scan lens and tube lens); and the focal length of the objective used (Fig. 2). A simple formula for the full FOV is:

$$FOV = 2 \times FL_{OBJ} \times \tan\left(SA \times \frac{FL_{SL}}{FL_{TL}}\right)$$

In this equation, SA is measured from the central optical axis, and is thus half of the full scan arc. Beam expansion is crucial because at the SE, smaller beam apertures can support increased scan speeds (higher temporal resolution), but large beam diameters are needed to overfill the back focal plane of the objective, which is critical for ensuring cellular resolution along the Z-axis (Zipfel et al., 2003; Kerr and Denk, 2008).

Next, we will discuss how the practical implementation of optics to support a large FOV involves careful engineering optimizations. Many of these essentially come down to accommodating high SAs using optical elements with short focal lengths (i.e., high numerical aperture [NA]) to ensure that the beam does not get clipped at any point in the system. In a representative two-photon microscope, the SA is ± 3.5°, the FL_{SL} = 50 mm, the FL_{TL} = 200 mm, and the FL_{OBJ} = 12.5 mm (Nikon CFI75, 16×, 0.8 NA). This would yield a total FOV of 380 µm.

Scanning system

A conventional scanning system consists of two galvanometer mirrors placed in proximity to one another, on orthogonal axes (to scan in X and Y). The deflection of the first mirror will cause displacement of the beam from the center of the second mirror. This

NOTES

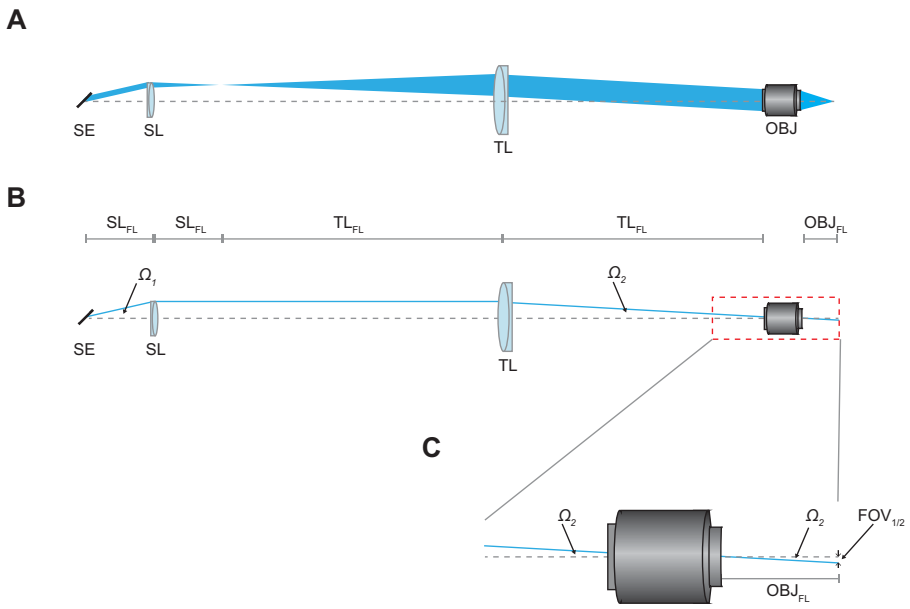

Figure 2. Basic optical layout for beam magnification after SE. *A,* After the SE, the deflected beam passes through the scan lens (SL) and then the tube lens (TL). This relay expands the beam and overfills the back aperture of the objective (OBJ). *B,* The distances between optics are configured in a 4f system. The final FOV is determined by the scanning angle (SA; Ω_2), which is determined by the SE SA (Ω_1), the ratio of the focal lengths of the SL and TL (this magnifies the beam and decreases the SA by reciprocal factors), and the focal length of the OBJ.

deflection is referred to as "beam walk." At low SAs (and when the FL_{SL} >> the distance between the two mirrors), this can be negligible (Tsai and Kleinfeld, 2009). However, at the relatively large SAs necessary for wide FOV imaging, beam walk can lead to a few millimeters of beam displacement on the second mirror, which can lead to beam clipping on either the scan lens, tube lens, or at the back focal plane of the objective. Any of these distortions would lead to vignetting and a reduction in the usable FOV. To combat this, an afocal relay can be placed between the *X* and *Y* scanning mirrors (Fig. 3). The afocal relay can be refractive (Kim et al., 1999; Vojnovic and Tullis, 2011) or reflective (Sharafutdinova et al., 2010a). In either case, high NA optics must be used to accept large SAs.

Scan lens

To increase the FOV, relatively high SAs are used. The scan lens must have a small enough *f*-number (i.e., sufficiently high NA) to accept these deflections. For SA = 10°, a scan lens of *f*-number ~2 (NA ~0.25) would be required. For a 1" diameter lens system, this translates to an effective focal length of 50 mm, to permit a 6 mm diameter beam to be scanned at ± 10°.

Beam expansion

The ratio of the focal lengths of the scan lens and the tube lens determine the beam expansion ratio (beam magnification = FL_{TL}/FL_{SL}). This expansion is needed to completely fill the back aperture of the objective; therefore, decreasing the beam expansion to increase the final entrance beam angle is not always practical. Once the scan-lens focal length is chosen, it will determine the focal length of the tube lens. For example, the back aperture on the widely used Nikon CFI75 16×/0.8 NA objective is ~22 mm. If the input beam is 6 mm (limited by the clear aperture of the scanning system), then a 4× beam expansion would overfill the back aperture of the objective.

Tube lens

Since the focal length of the scan lens and the beam expansion have been chosen, the focal length of the tube lens has been determined: In this case, it is 200 mm. Because the beam is undergoing expansion, when it reaches the tube lens, if the tube lens is not sufficiently large, the beam will be clipped. The center of the beam is displaced by (50 mm) * tan(10°) = ~9 mm. At the point it reaches the tube lens, the radius of the beam is 12 mm, and thus the minimum radius of the tube lens must be 9 mm + 12 mm = 21 mm; otherwise, significant vignetting will occur, limiting the usable FOV. In this case, 2" optics for the tube lens are sufficient. Often optomechanical components are placed between the tube lens and the objective (e.g., a 45° dichroic mirror to split excitation light and emitted fluorescence). All these elements must be large enough to prevent clipping of the beam

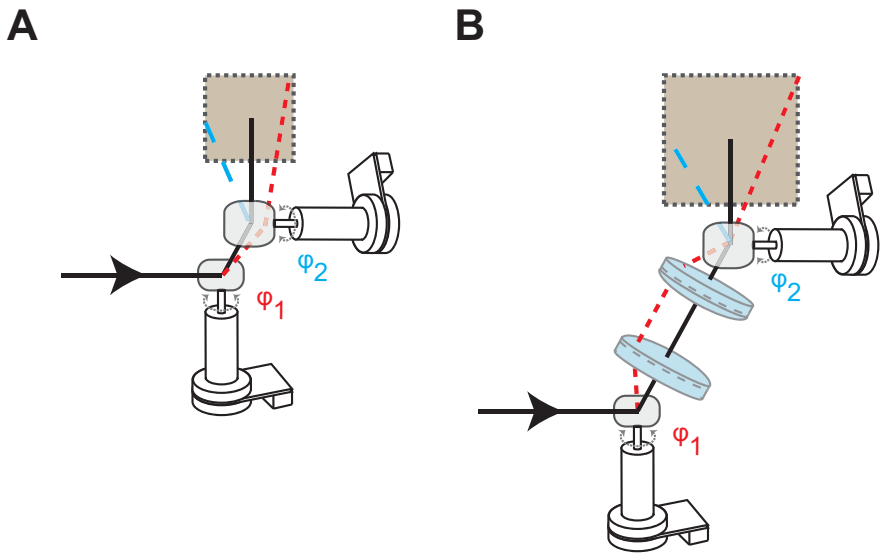

Figure 3. Beam walk. *A,* When scan mirrors are placed in proximity to one another, the deflection of the first mirror will cause displacement of the beam from the center of the second mirror. Called "beam walk," this can be negligible when scanning at small angles. However, at large angles, this leads to severe beam clipping and vignetting (a restricted FOV). *B,* To combat beam walk and maintain signal quality over larger scan angles (for a larger FOV), an afocal beam relay between the two scan mirrors can be used. Here, a refractive relay is shown. Reflective relays, using off-axis parabolic mirrors, can also be used.

even at high SA. Some long-focal-length custom objectives and high NA macroscope objectives have back apertures ~50 mm in diameter—more than twice what we considered in the present analysis. Although theoretically these objectives can provide a wide FOV, implementing them in a two-photon microscope (e.g., overfilling their back apertures) can present significant challenges.

Wavefront Considerations

In two-photon excitation, the scanning focal spot must be of high optical qualiwty and possess sufficient photon density to achieve two-photon excitation. Although high NA objectives are important, they are not always the limiting parameter when imaging over a large FOV. Optical aberrations, which can be introduced anywhere in the optical system, can degrade the wavefront and decrease the efficiency of two-photon excitation of a microscope. When scanning at small angles, aberrations can be minimal. However, aberrations become increasingly important at high scan angles, and these can ultimately limit the FOV. An extensive optimization study of scan and tube lens designs found that when using a single achromat for the scan lens, only approximately the central third of the theoretical FOV was diffraction-limited (Negrean and Mansvelder, 2014). This limitation is mainly the result of the significant astigmatism introduced at large off-axis angles. The usable fraction of FOV is increased with compound lens design (e.g., a Plossl lens) or completely custom scan lens systems. This study also showed that single achromats used for tube lenses can limit performance, whereas custom lens designs can again increase performance across the entire FOV (Negrean and Mansvelder, 2014).

The aberration-induced wavefront distortions must also be considered when using a relay between the scanning mirrors. Optimized relay lenses can be designed similarly to the scan lenses. The relay lenses must match the NA of the scan lens, or they will limit the usable angles. Another option is to use off-axis parabolic mirrors (Sharafutdinova et al., 2010a; Negrean and Mansvelder, 2014). Parabolic mirror–based relays can offer diffraction-limited performance across large SAs, and potentially provide lower wavefront errors compared with refractive designs or spherical mirror relays (Sharafutdinova et al., 2009, 2010a, b).

Once careful optical design has minimized most aberrations, adaptive optics can further improve performance by correcting residual aberrations, including those introduced by the preparation itself. *In vivo*, wavefronts cannot typically be measured directly; thus, various methods have been developed to determine patterns than can cancel aberrations during *in vivo* imaging and increase fluorescence yield (Debarre et al., 2009; Aviles-Espinosa et al., 2011; Ji et al., 2012).

NOTES

Imaging Speed

As the FOV increases in area, if the number of pixels per neuron is preserved, the quantity of effective pixels per image is greatly increased. For example, ≥100 neurons can be imaged in a 250 × 250 µm square FOV, and raster scanning requires at least 128 × 128 pixels (2^{14} pixels). Thus, for a 3 mm^2 image, ~4800 neurons can be imaged (though in practice, vasculature obscures a significant fraction of these), and $>2^{19}$ pixels can appear in a raster scan. For conventional galvanometer scanning, the scan speed is inertia-limited to ~1 kHz (1 ms/line). Since ~2^8 lines/frame are needed for a small region, this ultimately leads to a frame rate limit of ~10–15 frames per second for a 250 µm wide FOV. This rate limit can be sufficient for many experiments, as the dynamics for current GECIs are >100 ms, and even studies of spike-count correlations often use counting windows of 0.1–1.0 s. However, some experiments require (or can be enhanced by) higher scanning speeds. Moreover, scanning entire large FOVs can take several seconds per frame. Here we briefly survey some alternative approaches that can offer higher scan speeds.

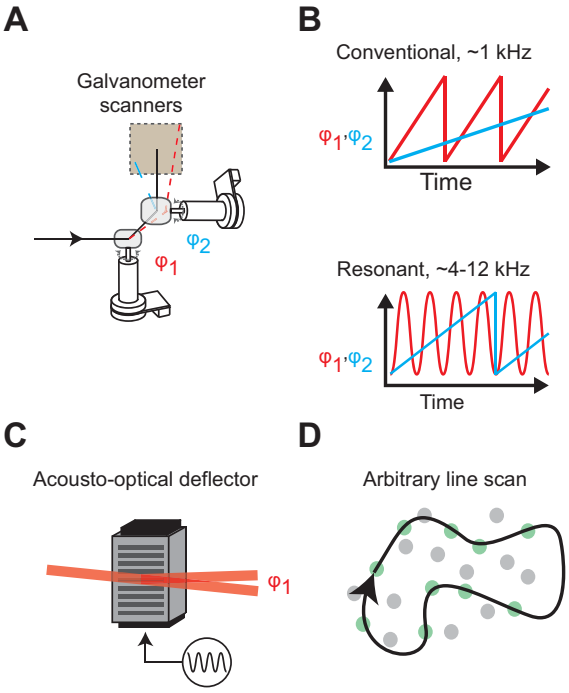

Figure 4. Beam SE technology. *A,* The most common SE is made from two galvanometer mirrors positioned along orthogonal axes. Scanning along one angle, φ_1, translates the beam along the *X*-axis, and scanning along the other angle, φ_2, translates the beam along the *Y*-axis. *B,* The basic driving waveform for dual galvanometer scanning is either a triangle or sawtooth (red) for the fast axis (typically the *X*-axis); the slower axis (*Y*-axis) is scanned using a sawtooth waveform (blue). When using a resonant scanner for the fast axis, the resulting scan is sinusoidal (red) at the fixed frequency of the resonant scanner. The slow axis is again scanned using a sawtooth waveform (blue). *C,* Another SE technology comprises AODs. These can be used in place of a galvanometer scanner for the fast axis, or multiple AODs can be used for 2D or 3D scanning. *D,* A faster alternative to raster scanning is arbitrary line scanning. Using either dual conventional galvanometers or AODs, a relatively short scan path can be defined that passes through cells of interest. This path can be retraced 10–100× faster than a conventional raster scan of the same area, thereby increasing temporal resolution.

Resonant scanning

Using a resonant scanner as the fast axis and a conventional galvanometer scanner as the slow axis, scan speeds of ≥30 frames/s are possible (Nguyen et al., 2001). The resonant axis oscillates at a fixed frequency (4–12 kHz), and thus the line scanning rate is fixed. Because the resonant scanner scans a sinusoidal path, resulting images need to be corrected for the nonlinearity. This correction can be done either by clipping the edges of the image (leaving the more linear central region) or by applying a nonlinear corrective procedure to the image (Haji-Saeed et al., 2007). Overall, resonant scanning systems can provide ample SAs, >20°, and thus are a good fit for wide FOV imaging.

Acousto-optical deflectors

An alternative method for achieving very high scan speeds employs acousto-optical deflectors (AODs; Fig. 4C). An AOD is a crystal whose angle of diffraction can be varied using an applied acoustic wave (typically in the radiofrequency range). An AOD can raster scan a laser beam at rates >100 Hz. Using AODs, fully three-dimensional (3D) noninertial scanning can be used to map neural activity (Duemani Reddy et al., 2008; Kirkby et al., 2010). The two drawbacks to AODs are added dispersion (which degrades two-photon excitation) and relatively small maximum SAs, typically <4°. While the former problem has been mostly solved, the latter issue remains, and demonstrated FOVs have been only ~700 µm across (Katona et al., 2012). Custom-designed AODs may offer increased SAs.

Arbitrary line scanning

When raster scanning, much of the FOV does not contain active neurons, and thus most of the pixels do not contain information that will be used by the experimenter. Thus, to increase the scan rate, one can utilize an arbitrary line scan (Fig. 4*D*). This can be supported by either conventional galvanometer scanners or AODs. In this method, a raster image is first acquired to obtain the position of all the cells of interest. Next, a scan path is generated in which the laser is directed to pass over each cell of interest. These scans can be optimized for speed and repeatability (Cotton et al., 2013).

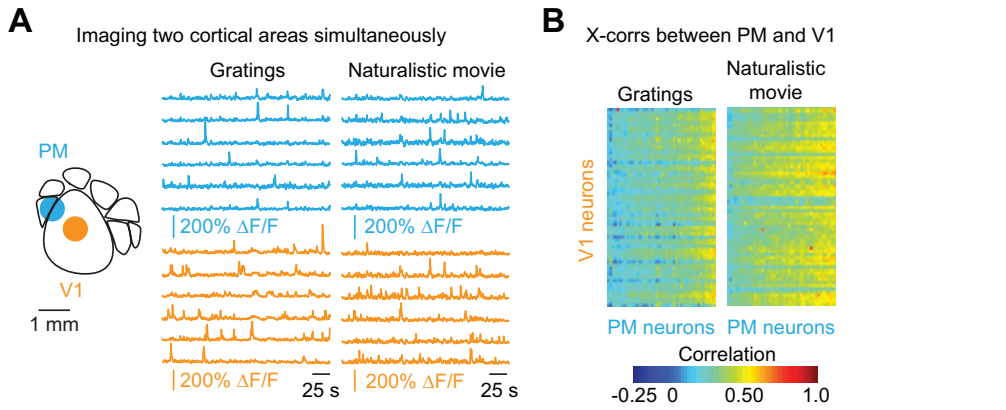

Figure 5. A solution for wide FOV imaging. ***A,*** Using a microscope with dual multiplexed beams and a wide FOV, cellular-level neural activity in two cortical areas (primary visual cortex and posteromedial [V1 and PM]) was imaged simultaneously. Signals for six neurons in each cortical area are shown. Scale bar, 1 mm. ***B,*** After deconvolving the fluorescence signals to obtain inferred spike rates, cross-correlations (X-corrs) were computed. X-corrs were higher during presentation of the naturalistic movie than during the drifting gratings. (The columns were ordered from low- to high-average correlation for presentation clarity.)

Multiplexed beam scanning

Any of the above methods can be combined for multiplexed beam scanning. In this approach, pulses from multiple beams are interleaved. Each beam scans a separate area, and fluorescence is collected using a single objective and focused onto a high-bandwidth detector. Synchronization pulses are used to determine which beam caused each florescence event. Because each beam can scan a separate area, the imaging speed scales up by a multiple of the number of beams used (Amir et al., 2007; Cheng et al., 2011).

Alternative Approaches

There are completely different approaches for imaging activity in multiple brain regions as well. For example, one could use two different microscopes. In this approach, the main challenge would be to place two objectives near one another, along with the rest of the optical pathways. However, with flexible positioning microscopes and low-profile objectives, it should be achievable, at a cost of increased complexity and likely limits on how close two imaged areas can be. Another simple solution would be to rapidly reposition the sample or the microscope. Movements of <1 mm can be achieved with a motorized stage in <0.5 s. Although this approach can be relatively simple to implement, it would suffer from severely limited maximal frame rates and low duty cycles (fraction of time spent imaging) owing to the movement time.

Our Solution

We have recently developed a two-photon microscope that can scan a wide FOV with cellular resolution. We utilized highly corrected, low *f*-number optics throughout the optical pathway to enable large FOV imaging: 1.4 mm with the Nikon CFI75 16 × 0.8 NA objective, and 3.5 mm with a custom-built objective. Because conventional raster scanning over the entire FOV area (>9 mm^2) can take 1–10 s per frame, we developed a version of beam multiplexing with dynamic beam-steering mirrors to support simultaneous scanning of two regions of interest (ROIs) anywhere within the overall FOV (Fig. 5). This method enables smaller ROIs to be scanned at ~5–30 frames/s yet still preserves the ability to have these regions widely separated within or across different cortical areas.

Conclusion

The FOV of two-photon imaging can be expanded to the mesoscale without sacrificing cellular resolution by minimizing optical aberrations and designing optomechanical systems that avoid limiting apertures. This technology will enable new kinds of experiments, in which dense samples of spatially separate populations of neurons are imaged nearly simultaneously. As a result, we will begin to map the distributed neural activity that underlies sensory processing and behavior in extended neural circuitry.

NOTES

References

Amir W, Carriles R, Hoover EE, Planchon TA, Durfee CG, Squier JA (2007) Simultaneous imaging of multiple focal planes using a two-photon scanning microscope. Opt Lett 32:1731–1733.

Aviles-Espinosa R, Andilla J, Porcar-Guezenec R, Olarte OE, Nieto M, Levecq X, Artigas D, Loza-Alvarez P (2011) Measurement and correction of *in vivo* sample aberrations employing a nonlinear guide-star in two-photon excited fluorescence microscopy. Biomed Opt Express 2:3135–3149.

Chen TW, Wardill TJ, Sun Y, Pulver SR, Renninger SL, Baohan A, Schreiter ER, Kerr RA, Orger MB, Jayaraman V, Looger LL, Svoboda K, Kim DS (2013) Ultrasensitive fluorescent proteins for imaging neuronal activity. Nature 499:295–300.

Cheng A, Goncalves JT, Golshani P, Arisaka K, Portera-Cailliau C (2011) Simultaneous two-photon calcium imaging at different depths with spatiotemporal multiplexing. Nat Methods 8:139–142.

Cotton RJ, Froudarakis E, Storer P, Saggau P, Tolias AS (2013) Three-dimensional mapping of microcircuit correlation structure. Front Neural Circuits 7:151.

Debarre D, Botcherby EJ, Watanabe T, Srinivas S, Booth MJ, Wilson T (2009) Image-based adaptive optics for two-photon microscopy. Opt Lett 34:2495–2497.

Denk W, Strickler JH, Webb WW (1990) Two-photon laser scanning fluorescence microscopy. Science 248:73–76.

Duemani Reddy G, Kelleher K, Fink R, Saggau P (2008) Three-dimensional random access multiphoton microscopy for functional imaging of neuronal activity. Nat Neurosci 11:713–720.

Haji-Saeed B, Khoury J, Woods CL, Pyburn D, Sengupta SK, Kierstead J (2007) Mapping approach for image correction and processing for bidirectional resonant scanners. Opt Eng 46:027007.

Ji N, Sato TR, Betzig E (2012) Characterization and adaptive optical correction of aberrations during *in vivo* imaging in the mouse cortex. Proc Natl Acad Sci USA 109:22–27.

Katona G, Szalay G, Maak P, Kaszas A, Veress M, Hillier D, Chiovini B, Vizi ES, Roska B, Rózsa B (2012) Fast two-photon *in vivo* imaging with three-dimensional random-access scanning in large tissue volumes. Nat Methods 9:201–208.

Kerr JN, Denk W (2008) Imaging *in vivo*: watching the brain in action. Nat Rev Neurosci 9:195–205.

Kim KH, Buehler C, So PT (1999) High-speed, two-photon scanning microscope. Appl Opt 38:6004–6009.

Kirkby PA, Srinivas Nadella KM, Silver RA (2010) A compact Acousto-Optic Lens for 2D and 3D femtosecond based 2-photon microscopy. Opt Exp 18:13721–13745.

Negrean A, Mansvelder HD (2014) Optimal lens design and use in laser-scanning microscopy. Biomed Opt Exp 5:1588–1609.

Nguyen QT, Callamaras N, Hsieh C, Parker I (2001) Construction of a two-photon microscope for video-rate Ca(2+) imaging. Cell Calcium 30:383–393.

Sharafutdinova G, Holdsworth J, van Helden D (2009) Improved field scanner incorporating parabolic optics. Part 1: Simulation. Appl Opt 48:4389–4396.

Sharafutdinova G, Holdsworth J, van Helden D (2010a) Improved field scanner incorporating parabolic optics. Part 2: Experimental verification and potential for volume scanning. Appl Opt 49:5517–5527.

Sharafutdinova G, Holdsworth J, van Helden D (2010b) Calculated two-photon fluorescence correction factors for reflective scan engines. Appl Opt 49:1472–1479.

Tsai PS, Kleinfeld D (2009) *In vivo* two-photon laser scanning microscopy with concurrent plasma-mediated ablation. In: Methods for *in vivo* optical imaging, Vol 3 (Frostig R, ed.), pp. 59–115. Boca Raton, FL: CRC Press.

Vojnovic B, Tullis ID (2011) Optical laser beam scanner lens relay system. © Gray Institute, Department of Oncology, University of Oxford. http://goo.gl/IqZa1W.

Zipfel WR, Williams RM, Webb WW (2003) Nonlinear magic: multiphoton microscopy in the biosciences. Nat Biotech 21:1369–1377.